IJC
International Journal of Cancer

Quantitative, qualitative and spatial analysis of lymphocyte infiltration in periampullary and pancreatic adenocarcinoma

Sebastian Lundgren [1], Jacob Elebro[1], Margareta Heby[1], Björn Nodin[1], Karin Leandersson[2], Patrick Micke[3], Karin Jirström[1] and Artur Mezheyeuski[3]

[1]Department of Clinical Sciences Lund, Division of Oncology and Pathology, Lund University, Lund, Sweden
[2]Department of Translational Medicine, Division of Cancer Immunology, Lund University, Lund, Sweden
[3]Department of Immunology, Genetics and Pathology, Uppsala University, Uppsala, Sweden

Immunotherapeutic modalities are currently revolutionizing cancer treatment. In pancreatic cancer, however, early clinical trials have been disappointing. The optimization of immunotherapeutic strategies requires better understanding of the inflammatory tumor microenvironment. Therefore, the aim of our study was to perform a detailed *in situ* description of lymphocyte infiltration patterns in resected pancreatic and other periampullary cancers. Multiplexed immunofluorescence imaging was applied to tissue microarrays with tumors from a cohort of 175 patients with resected periampullary adenocarcinoma. A panel of immune cell markers including CD4, CD8α, FoxP3, CD20, CD45RO and pan-cytokeratin was applied to allow for simultaneous spatial analysis of multiple lymphocyte populations. The majority of lymphocyte populations were significantly more abundant in intestinal (I-type) compared to pancreatobiliary (PB-type) tumors. Hierarchical cluster analysis revealed several immune cell signatures of potential clinical relevance. Notably, in the stromal compartment of PB-type tumors, high infiltration of B cells, $CD8\alpha^+CD45RO^+$ and single-positive $CD4^+$ T cells, but low levels of $FoxP3^+CD45RO^{high}$ and single-positive $CD8\alpha^+$ T cells were associated with improved overall survival (OS). The study also defined prognostic relevant topographical patterns of lymphocytic infiltration, in particular proximity of $CD8\alpha^+$ cells to cancer cells. Moreover, the presence of lymphocytes with potential T-helper capacities ($CD4^+$) in the nearest vicinity to $CD8\alpha^+$ cells was associated with a prolonged OS. Our data demonstrate that the composition and clinical impact of immune infiltrates in periampullary adenocarcinoma differ by morphological type as well as localization. Furthermore, spatial *in situ* analysis identified potential immunological mechanisms of prognostic significance.

Introduction

Periampullary adenocarcinoma, including pancreatic cancer, is a collective term for cancers arising around the ampulla of Vater. The periampullary region is a complex region which is composed of distinct anatomical structures: the head of the pancreas, distal common bile duct, second portion of the duodenum and ampulla of Vater. Periampullary adenocarcinomas are currently classified by their anatomic location of origin according to the seventh edition of the American Joint Committee on Cancer staging system.[1] They can be divided into two subgroups based on morphology, either intestinal type (I-type) or pancreatobiliary type (PB-type), and there is increasing evidence that morphology is a more important determinant of survival than anatomical origin.[2–5] Survival rates remain dismally low for this group of patients, with 5-year overall survival (OS) rates of around 6%,[6] partly due to late presentation of the disease, but also because both conventional and targeted therapies have shown limited efficacy. Currently, the only curative treatment of pancreatic and periampullary adenocarcinomas is surgery, however, only 15–20% of the patients are eligible for surgery at the time of

Additional Supporting Information may be found in the online version of this article.

Key words: periampullary cancer, pancreatic cancer, lymphocytes, T cells, B cells

Abbreviations: DAPI: 4′,6-diamidino-2-phenylindole; dMMR: deficient mismatch repair; HR: hazard ratios; I-type: intestinal- type; MSI: microsatellite instable; OS: 5-year overall survival rates; PB-type: pancreatobiliary type; pMMR: proficient mismatch repair; TILs: tumor-infiltrating lymphocytes; Tregs: regulatory T cells; wt: wild-type

DOI: 10.1002/ijc.32945
History: Received 8 Nov 2019; Accepted 21 Feb 2020; Online 4 Mar 2020

Correspondence to: Sebastian Lundgren, E-mail: sebastian.lundgren@med.lu.se

What's new?

Immunotherapy has revolutionized the treatment of multiple cancer types, including certain digestive tract malignancies, such as stomach and colorectal cancer. Pancreatic and other periampullary cancers, however, have eluded immunotherapeutic strategies, likely owing to the highly complex tumor microenvironment of these cancers. Indeed, in this study, analyses of a retrospective series of resected human periampullary adenocarcinomas show that lymphocyte infiltration varies significantly according to tumor compartment and mutational status. The authors also identified significant associations between survival and different immune cell infiltration signatures, furthering the idea that infiltrating immune cells serve a critical role in clinical outcome.

diagnosis.[7] Chemotherapy regimens such as gemcitabine and FOLFIRINOX are used in the adjuvant setting with limited survival gains,[8–10] and immunotherapies have thus far shown little promise.

One of the hallmarks of cancer is its ability to evade destruction by the immune system,[11] and tumor-infiltrating immune cells play an integral role in shaping the tumor microenvironment.[12] The role of immune cells in the tumor microenvironment is however complex and dependent upon a multitude of factors such as tumor type, cellular interactions, leukocyte plasticity as well as their localization within the microenvironment itself. There is ample evidence that the location and density of infiltrating immune cells play an important role in the clinical outcome for cancer patients.[13,14]

Pancreatic cancer harbors high levels of immuno-suppressive leukocyte populations, such as T regulatory cells (T-regs) and tumor-associated macrophages with tolerogenic phenotypes, enabling tumor progression.[15] Additionally, the stromal composition of pancreatic cancer seems to depend upon infiltrating leukocyte profiles,[16] adding more evidence to the importance of these cells in determining the biology of pancreatic cancer. The complex interactions in the tumor microenvironment lead to an immune-privileged disease, with low immunogenicity. Additionally, the mutational burden of pancreatic cancer is comparatively low, leading to low antigenicity, which further limits the immune response.[17,18] However, there seem to be subsets of patients with pancreatic cancer with functional antitumoral immune cell response.[19,20] Hence, a deeper understanding of the multifaceted role of different immune cell populations in pancreatic and periampullary adenocarcinomas is needed.

Although there is accumulating evidence that the composition of tumor immune cell infiltrates is of major importance, many observations are inconsistent. Most previous studies rely on single markers rather than combinations thereof, disregarding the reciprocal interaction of immune cells. Moreover, the spatial localization of the immune cells appears to bear relevance,[21] and the coappearance of cytotoxic immune cells and cancer cells has recently been recognized as a predictor of response to immunotherapy.[22,23]

The aim of our study was therefore to map the spatial distribution and perform a comprehensive phenotyping of important lymphocyte populations in the tumor microenvironment of pancreatic and periampullary adenocarcinomas, with particular reference to tumor morphology and patient outcome.

Methods

Study cohort

The study cohort consists of a retrospectively collected consecutive series with primary tumors from 175 incident patients who underwent pancreaticoduodenectomy for periampullary adenocarcinoma in the University hospitals of Lund and Malmö from January 1, 2001 to December 31, 2011.[24,25] Approval for the study was obtained from the Ethics committee of Lund University (reference number 445/07), whereby the committee waived no need for consent other than the option to opt-out. Follow-up started at the date of surgery and ended at death or on March 31, 2017, whichever came first. The Swedish National Civil Register was used to obtain information on vital status. Data on adjuvant treatment were obtained from patient charts. All cases underwent strict histopathological re-evaluation by a board-certified pathologist (JE). Sixty-five tumors were classified as intestinal type (I-type), and 110 as pancreatobiliary-type (PB-type), whereof the anatomical origin of the tumors was 14 duodenal, 70 ampullary, 45 distal bile duct and 46 pancreatic. In 63 cases, paired-samples from lymph node metastases were available, 21 from I-type tumors and 42 from PB-type tumors. In 34 cases, paired-samples from benign tissue was available, 9 from I-type tumors and 25 from PB-type tumors. Mismatch repair status was assessed by immunohistochemistry as previously described.[26]

Tissue microarray construction

Tissue microarrays were constructed as previously described,[27,28] using a semi-automated arraying device (TMArrayer, Pathology Devices, Westminister, MD). Three 1 mm cores were sampled from viable, non-necrotic areas of the primary tumors. Four-micrometer TMA-sections were then used in the subsequent immunofluorescence staining.

Multiplex immunohistochemical staining

Multiplexed immunofluorescence staining was performed using the Opal Multiplex IHC Kit (PerkinElmer, Waltham, MA). A panel of immune markers was developed with antibodies against CD4 (Mouse/4B12, DAKO/M7310, 1:200), CD8α (Mouse/144B, Thermo Fisher Scientific/MA5-13473, 1:500), FoxP3 (Rabbit/D6O8R, Cell Signaling Technology/12653s, 1:100), CD20 (Mouse/

L26, DAKO/GA604, 1:3,000) and CD45RO (Mouse/UCHL1, Thermo Fisher Scientific/MA1-19452, 1:200). For pan-cytokeratin staining, a combination of several antibodies was used: anti-E-cadherin (Mouse/Clone 36, BD Biosciences/610182, 1:5,000), anti-pan Cytokeratin (Mouse/[C-11], Abcam, San Francisco/ab7753, 1:1,000) and anti-pan Cytokeratin Clone, 1:2,000 (Mouse/AE1/AE3, Thermo Fisher Scientific/MA5-13156, 1:500). To visualize cell nuclei, the tissue was stained with 4′,6-diamidino-2-phenylindole (Spectral DAPI, PerkinElmer). The staining procedure was largely performed as previously described.[29]

Imaging

Imaging of the TMAs was performed with the Vectra Polaris system (PerkinElmer). First, a whole slide scan at 10× magnification was acquired for TMA core annotation and selection of regions on which to apply multispectral imaging. Multispectral imaging was then performed at a resolution of 2 pixels per 1 μm. Spectral unmixing was carried out using inForm software (PerkinElmer).

Image analysis and thresholding

First, image analysis was performed with the inForm Analysis software (PerkinElmer), wherein each scanned image was visually assessed by a board-certified pathologist (PM) to exclude large areas of nontumor tissue, cores without tumor tissue, necrosis or artifacts from the analytical process. After this, image analysis was performed in two steps; a training session and an image analysis session. In the training session, a set number of cores were categorized into three types of tissue compartment: tumor compartment (or epithelial compartment in non-malignant samples), stromal compartment, or blank areas. A machine-learning algorithm then carried out tissue segmentation (Supporting Information Fig. S1).

Cell segmentation was carried out as described before.[29] In short, DAPI staining was used to segment cells. The perinuclear area was defined as a 3-μm (6 pixels) area surrounding nuclei and was therefore considered to be cell cytoplasm. The total cell area, including nuclear and cytoplasmic areas, was evaluated for cytoplasmic/membrane marker expression. FoxP3 expression was evaluated in nuclear (DAPI positive) areas only. Additionally, coordinates on the *y* and *x*-axis were retrieved for each individual segmented cell. Lymphocyte infiltration was normalized against the area of viable tissue in each core.

The inForm built-in function for cell phenotyping was used to define the intensity threshold for the positivity of each marker individually, using a random selection of TMA cores. The defined thresholds were then applied for the raw output data of the complete cohort. Thus, each cell was characterized by positivity–negativity of each marker. The co-expression data was then used to identify immune cell subtypes.

Immune cell infiltration was evaluated as the number of cells per region, in the stromal compartment, tumor compartment or total viable tissue area of the TMA cores, respectively.

Cell spatial localization was assessed in two ways: to evaluate the relation of immune cells to tumor tissue, the distance of each cancer cell (defined as cytokeratin single-positive cells) to its nearest neighboring immune cell (of each subclass separately) was measured. A median distance value was computed for each case. The potential interaction zone between lymphocytes and/or cancer cells used in the interaction analyses was set to a radius of 15 μm.

Next-generation DNA sequencing

Next-generation DNA sequencing was performed as previously described.[5] In brief, tissue cores were taken from tumor enriched areas. DNA was extracted using the Qiagen GeneRead (Qiagen, Hilden, Germany) kit for formalin-fixed paraffin-embedded tissue according to the instructions from the manufacturer. In total, 102 (58.3%) cases had a sufficient number of tumor cells for analysis. A panel of 70 cancer-associated genes was characterized using Illumina TruSeq custom amplicon assay (Illumina, San Diego, CA) with a MiSeq instrument according to the instructions from the manufacturer. Variant calling and annotation, quality filtering and alignment were performed using the supplier's analysis pipeline. To exclude single-nucleotide polymorphisms commonly reported in various populations, detected mutations were screened against the COSMIC and ExAC databases.

Data processing and statistical analyses

For comparison of two groups of related samples, Wilcoxon signed-rank test with Pratt modification was used. Kruskal–Wallis test was used for comparison of multiple groups. Unsupervised hierarchal clustering was performed on normalized data to identify immune cell signatures. Kaplan–Meier analysis and log-rank test were applied to illustrate any difference in 5-year OS and Cox regression proportional hazard models were used to estimate hazard ratios (HR) for death within 5 years in both univariable and multivariable analyses. Multivariable Cox regression included adjustment for age (continuous), T-stage (T1–T2 *vs.* T3–T4), N-stage (negative *vs.* positive nodal status), grade (well-moderate *vs.* poor), adjuvant chemotherapy (none *vs.* any), invasion into vascular and lymphatic structures and perineural growth. Morphology (I-type *vs.* PB-type) was included in the multivariable model in analyses of the entire cohort.

In the entire cohort, three cases were excluded in the survival analyses; one patient with a PB-type tumor who was lost to follow-up due to emigration, and two patients with I-type tumors who died of complications from the initial surgical treatment within the first month.

All statistical calculations were performed with SPSS version 24.0 (SPSS Inc, Chicago, IL) or with R software, version 3.3.3 (R Foundation for Statistical Computing, Vienna, Austria) and integrated development environment RStudio, version 1.0.143 (RStudio Team, Boston, MA). All statistical tests were two-sided and p values <0.05 were considered significant.

Data availability

The data that support the findings of our study are available from the corresponding author upon reasonable request.

Results

Expression patterns of immune markers

Immune cell infiltration was possible to determine in 161 (92%) of the cases, whereof 63 were I-type and 98 were PB-type tumors. A representative example of a multiplex immunofluorescent image is shown in Figure 1*a*. Individual marker expression levels in each cell were used to identify TIL subtypes: $CD4^+$ single-positive cells (negative for all markers except CD4), $CD4^+CD45RO^+$cells (referred to as activated $CD4^+$ cells; memory $CD4^+$ T cells may be included in this population), $CD4^+FoxP3^+$ (referred to as $CD4^+$ Treg cells), single-positive $CD8^+$ cells (negative for all markers except CD8α), $CD8\alpha^+CD45RO^+$ (referred to as activated

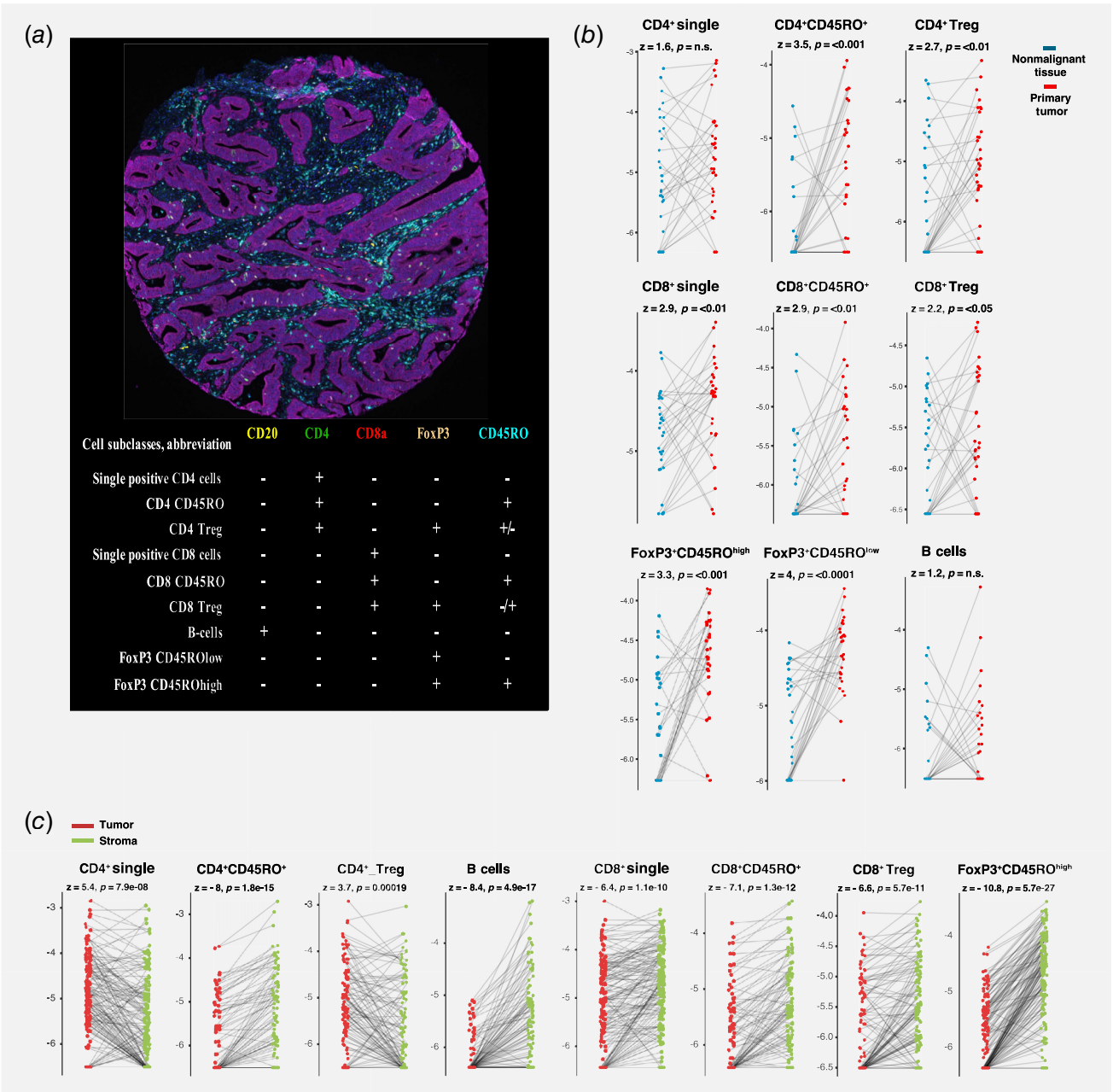

Figure 1. Heterogeneity of the infiltration of lymphocyte subpopulations in periampullary adenocarcinoma. (*a*) *Upper part*: Representative image of a TMA core with heterogeneous infiltration of lymphocytes. *Lower part*: summarized scheme of the five immune marker combinations, used to define subpopulations of lymphocytes. (*b*) Immune cell densities in primary tumor and adjacent nonmalignant tissue. (*c*) Immune cell densities in tumor *versus* stromal compartment in primary tumor tissue. [Color figure can be viewed at wileyonlinelibrary.com]

$CD8^+$ cells; memory $CD8^+$ T cells may be included in this population), $CD8\alpha^+FoxP3^+$ (referred to as $CD8^+$ Treg cells), $FoxP3^+CD45RO^{low}$, $FoxP3^+CD45RO^{high}$ and single $CD20^+$ cells (referred to as B cells; Fig. 1*a*).

We also observed nuclear expression of FoxP3 in a fraction of tumor cells. This feature has been reported before,[30,31] and was not considered in the analyses. Interestingly, in the stromal compartment we also observed $FoxP3^+$ cells that were negative for CD4 or CD8α. These cells were either $CD45RO^{high}$ or $CD45RO^{low}$ and may therefore at least in part be γδ T cells or NKT cells that lack CD4 and CD8α expression (Supporting Information Fig. S2). Since $FoxP3^+CD45RO^{low}$ cells were difficult to distinguish from $FoxP3^+$ cancer cells in the tumor compartment, the analysis of $FoxP3^+CD45RO^{low}$ lymphocytes was restricted to the stromal compartment.

The heterogeneity of the immune landscape in tumors and nonmalignant tissue

First, we compared lymphocyte infiltration in cancer tissue and adjacent nonmalignant tissue in a pairwise manner. All of the lymphocyte subclasses, except single-positive CD4 cells and B cells, were more abundant in malignant tissue (Fig. 1*b*).

Next, we performed a pairwise comparison of lymphocyte infiltrates within the tumor and stromal compartments in samples with cancer tissue (Supporting Information Fig. S1). As illustrated in Figure 1*c*, densities of B cells and all $CD8\alpha^+$ lymphocyte subclasses were significantly higher in the stromal compared to the tumor compartment. $CD4^+$ cells exhibited a different infiltration pattern in that $CD4^+CD45RO^+$ T cells were more abundant in the stromal compartment, whereas single-positive CD4 cells and $CD4^+$ Tregs were enriched in the tumor compartment.

Associations of lymphocyte infiltration with tumor morphological type, anatomical origin and clinicopathological characteristics

The relative proportion of TIL subclasses, stratified by tumor morphology, is shown in Figure 2*a*. The most abundant cell subclasses in the total tissue area, and the tumor compartment, were single-positive $CD4^+$ and single-positive $CD8^+$ cells. The most abundant TIL subpopulations in the stromal compartment were single-positive $CD8^+$ cells and $FoxP3^+CD45RO^{low}$ cells. No significant differences were observed between I-type and PB-type tumors with regard to total lymphocyte count. However, when the tumor compartment was analyzed separately, levels of $CD4^+CD45RO^+$ T cells ($p = 0.027$) were significantly higher in PB-type tumors, while levels of $CD8^+CD45RO^+$ T cells ($p < 0.001$), $CD8^+$ Tregs ($p = 0.001$), $FoxP3^+CD45RO^{high}$ cells ($p = 0.004$) and B cells ($p = 0.011$) were significantly higher in I-type tumors (Fig. 2*a*). In the stromal compartment, levels of $FoxP3^+CD45RO^{low}$ cells ($p = 0.004$) and $FoxP3^+CD45RO^{high}$ cells ($p = 0.026$) were significantly higher in I-type tumors (Fig. 2*a*). These data indicate a link between tumor histology and lymphocyte infiltration patterns. This was further investigated by analyzing lymphocyte densities in strata according to anatomical localization (Fig. 2*b*). Notably, tumors with pancreatic origin displayed lower densities of all analyzed lymphocyte subclasses, including those with potential immune suppressive activity, in both the tumor and stromal compartments, while duodenal cancers had the all-over highest lymphocyte infiltration (Fig. 2*b*).

Finally, we compared lymphocyte infiltration with clinicopathological characteristics. Lower densities of most analyzed lymphocyte subclasses were observed in tumors with positive resection margins, presence of perineural growth, invasion in lymphatic and blood vessels and growth in peripancreatic fat (Fig. 2*c*). Altogether, these data suggest that lower levels of infiltrating lymphocytes are associated with adverse clinicopathological characteristics.

Lymphocyte infiltration in relation to the mutational landscape and mismatch repair status

The relationship between different immune cell populations and the most common mutations (≥10% prevalence) are shown in Supporting Information Figure S3. Notably, the infiltration of several $CD8^+$ cell populations, both in the tumor and stromal compartments, was significantly lower in *KRAS* mutated compared to *KRAS* wild-type (wt) tumors. The infiltration of different immune cells subsets did also differ significantly according to mutational status of *SMAD4*, *CDK2NA*, *APC*, but not of *TP53*, *RNF43*, *SMARCA4*, *ERBB3* or *NF1*.

As shown in Supporting Information Figure S4, the infiltration of several immune cell populations was significantly higher in I-type tumors with deficient mismatch repair (dMMR) status. In PB-type tumors there was no association between dMMR status and lymphocyte infiltration, however, the infiltration of $FoxP3^+CD45RO^{low}$ lymphocytes was higher in tumors with proficient mismatch repair (pMMR).

Associations of lymphocyte infiltration with survival

For survival analysis, tumors were dichotomized into two groups with high or low lymphocyte infiltration using the median values as cut-off.

As shown in Supporting Information Figure S5, the total density of all lymphocyte subpopulations, except for single-positive CD8 cells, $CD8^+$ Tregs and $FoxP3^+CD45RO^{high}$ cells, inferred a prognostic value, positive or negative, in univariable Cox regression analysis of the entire cohort. In multivariable analysis, single-positive CD4 cells (HR = 0.53, 95% CI 0.36–0.79), $CD8^+CD45RO^+$ T cells (HR = 0.58, 95% CI 0.40–0.87) and B cells (HR = 0.54, 95% CI 0.37–0.80) remained significantly associated with a prolonged OS. In I-type tumors, none of the lymphocyte subpopulations conferred an independent prognostic value, whereas, in PB-type tumors, a high density of $CD8^+CD45RO^+$ T cells was an independent predictor of a prolonged OS (HR = 0.54, 95% CI 0.34–0.88).

As further shown in Supporting Information Figure S5, survival analyses restricted to the tumor compartment revealed that only single-positive CD4 cells were significantly

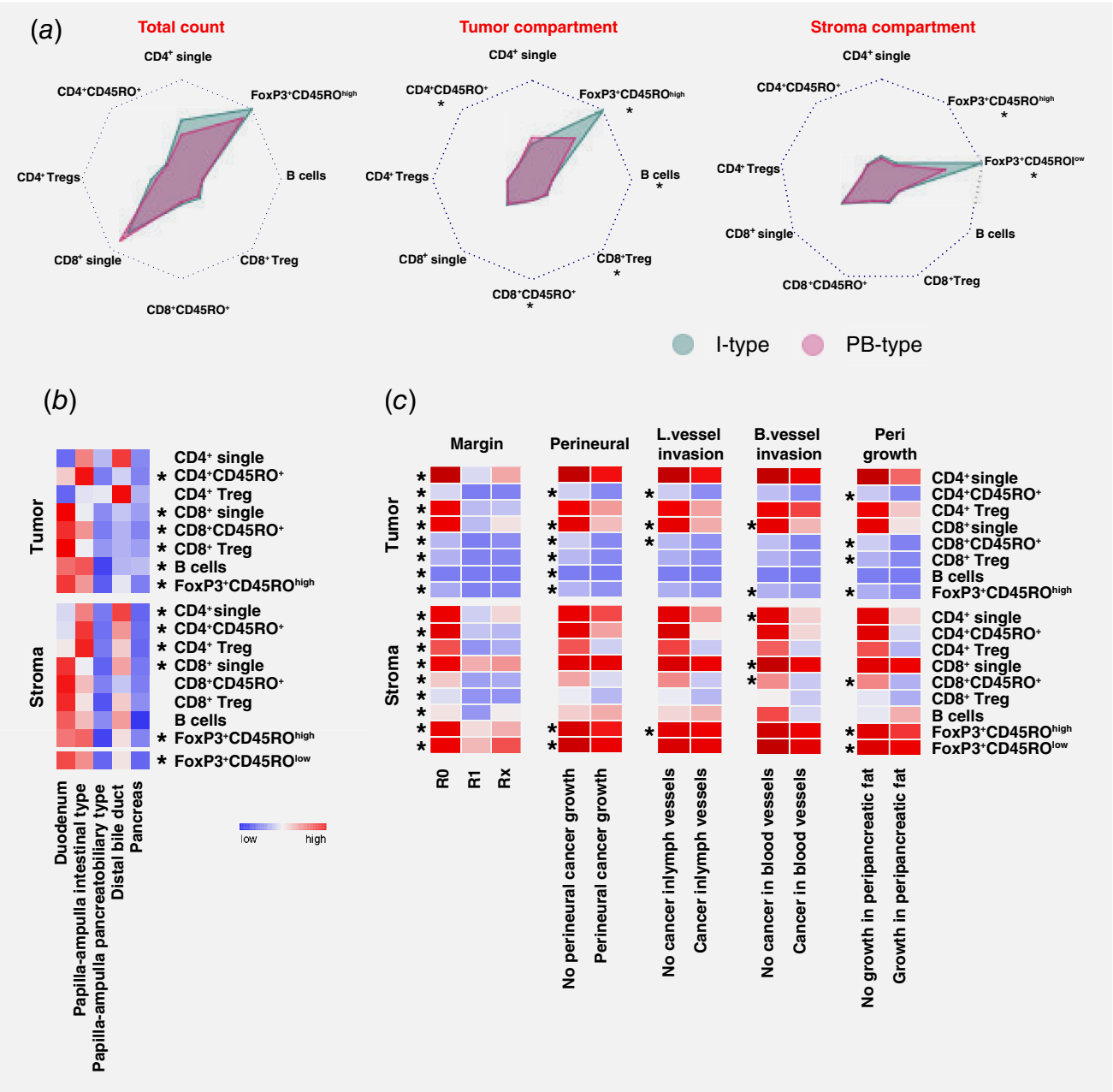

Figure 2. Heterogeneity of lymphocyte infiltration patterns associated with tumor morphological type, anatomical origin and clinicopathological characteristics. (*a*) Radar plots of relative densities of immune cell subclasses in PB-type tumors (purple) and in I-type tumors (blue), shown separately for total tissue, tumor compartment and stromal compartment. (*b*) Heat map of the densities of immune cell subclasses in tumor and stromal compartments according to the anatomical origin. (*c*) Heat maps illustrating the associations between the densities of immune cell subclasses and clinicopathological characteristics. [Color figure can be viewed at wileyonlinelibrary.com]

associated with OS in multivariable analysis (HR = 0.61, 95% CI 0.41–0.91) in the entire cohort. Survival analyses restricted to the stromal compartment revealed that single-positive CD4 cells and B cells were independent predictors of a prolonged OS (HR = 0.62, 95% CI 0.42–0.92 and HR = 0.57, 95% CI 0.39–0.84) in the entire cohort. No significant associations were found between single lymphocyte populations and survival when stratifying for morphology.

Tumor to stroma ratios of infiltrating lymphocytes and their associations with survival

In the next set of analyses, we aimed to distinguish "inflamed" and "immune excluded" tumors. As illustrated in Figure 3*a*, tumors with an active anticancer immune response (inflamed) are expected to have an enrichment of lymphocyte infiltration in the tumor nest, while "immune excluded" tumors are characterized by an accentuation of lymphocyte infiltration in the

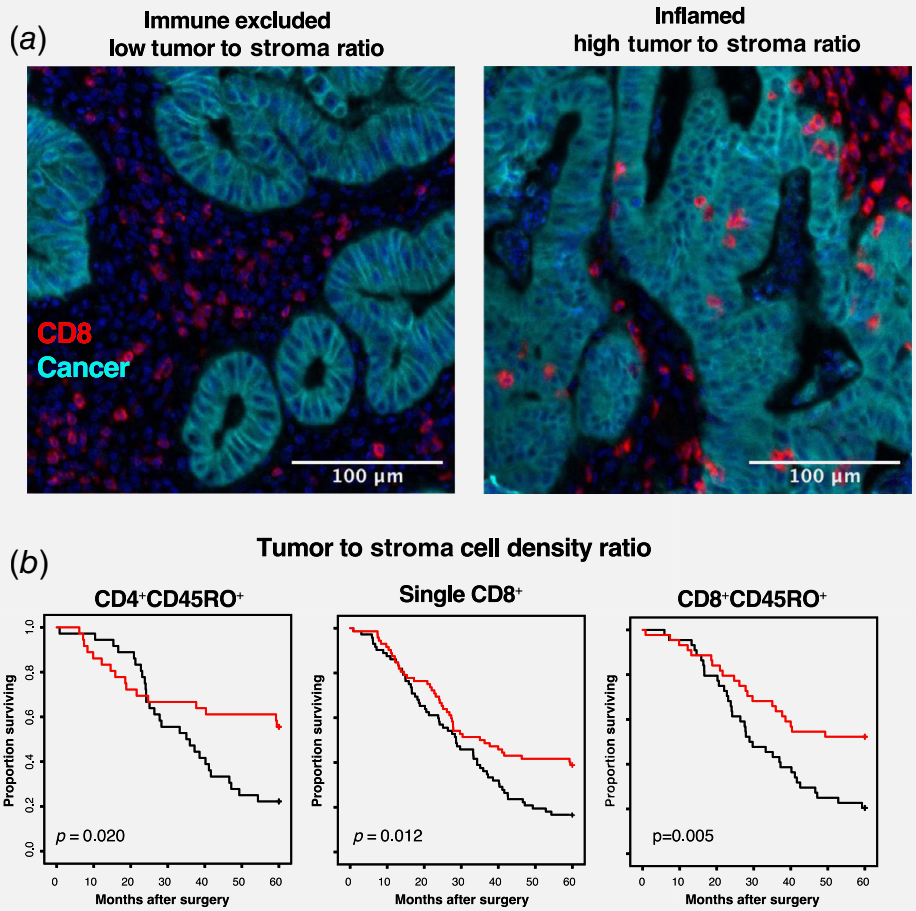

Figure 3. Inflamed *versus* immune excluded immunophenotypes. (*a*) Representative images illustrating the concept of immune inflamed and immune-excluded infiltration patterns of $CD8^+$ cells. (*b*) Kaplan–Meier analysis of 5-year OS in relation to the ratio between intratumoral and stromal immune infiltrates. [Color figure can be viewed at wileyonlinelibrary.com]

stromal compartment. A "Tumor to Stroma Ratio" metric was generated by dividing the density of lymphocyte infiltration in the tumor compartment with the density of lymphocyte infiltration in the stromal compartment. The tumors were subsequently dichotomized into two groups with high or low Tumor to Stroma ratio using the median values as cut-off. As shown in Figure 3*b*, high Tumor to Stroma Ratios of $CD4^+CD45RO^+$ T cells, single-positive CD8 cells and $CD8^+CD45RO^+$ T cells were associated with a prolonged OS. These associations were confirmed in univariable analysis (HR = 0.48, 95% CI 0.25–0.90, HR = 0.62, 95% CI 0.42–0.92 and HR = 0.44, 95% CI 0.25–0.76, respectively). However, in multivariable analysis, only a high Tumor to Stroma Ratio of single-positive CD8 cells remained significantly associated with a prolonged OS (HR = 0.64, 95% CI 0.41–0.99). No significant associations with survival were found in univariable analysis when stratifying for morphology. In PB-type tumors, however, the Tumor to Stroma Ratio of single-positive CD8 cells was significantly associated with a prolonged OS in multivariable analysis (HR = 0.50, 95% CI 0.29–0.86).

Lymphocyte infiltration patterns and their associations with survival

When cases were clustered according to total count of TIL density, seven distinct immune cell signatures were defined (Supporting Information Fig. S6). Kaplan–Meier analysis revealed that immune signature 1, characterized by high levels of $CD4^+CD45RO^+$ T cells, $CD8^+CD45RO^+$ T cells, $FoxP3^+CD45RO^{high}$ cells, but low levels of single-positive CD4 and CD8 cells, was significantly associated with a prolonged OS compared to immune signatures 3 and 6 ($p = 0.027$ and $p = 0.022$, respectively; Supporting Information Fig. S7). These associations were confirmed in unadjusted Cox regression analysis (HR = 3.18, 95% CI 1.00–9.17 and HR = 3.32, 95% CI 1.14–9. 66, respectively), but did not remain significant in adjusted analysis. When stratified for morphology, no immune cell signatures were significantly associated with OS.

Six distinct tumor nest (TN) immune cell signatures were defined. Kaplan–Meier analysis revealed that in the entire cohort, TN immune signature 3, characterized by high levels of $FoxP3^+CD45RO^{high}$ cells, and $CD8^+CD45RO^+$ T^-cells (Fig. 4*a*), was significantly associated with a prolonged OS compared to TN

immune signature 2 (p = 0.003; Supporting Information Fig. S7). In unadjusted Cox regression analysis using TN immune signature 3 as reference, TN immune signature 2 (HR = 3.65, 95% CI 1.45–8.61), TN immune signature 5 (HR = 2.47, 95% CI 1.08–5.62) and TN immune signature 6 (HR = 2.64, 95% CI 1.16–6.01) were significantly associated with a reduced

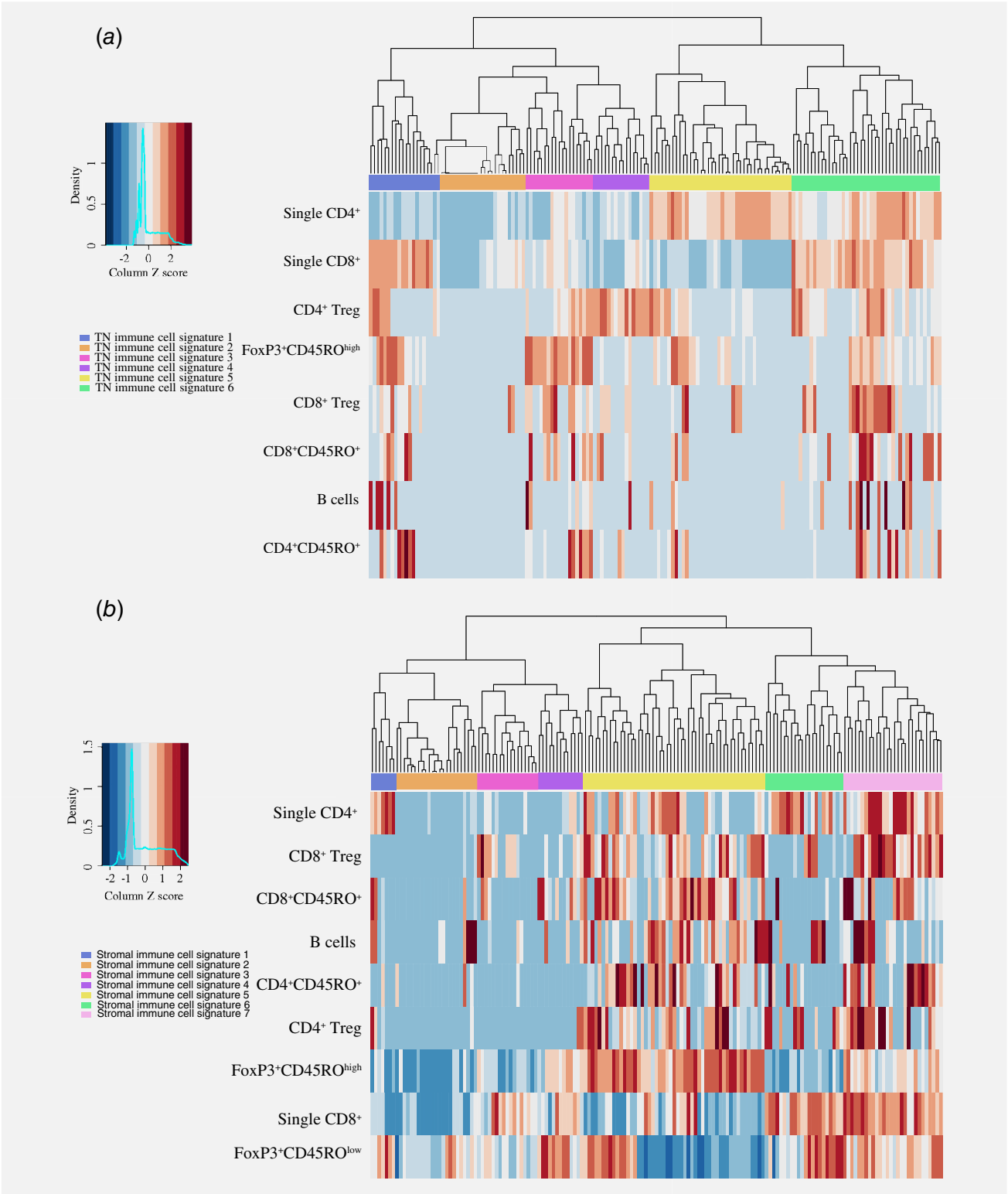

Figure 4. Identification of immune cell signatures by hierarchical clustering. Heatmaps illustrating hierarchical clustering of cases by normalized densities of lymphocyte infiltration rates in the (*a*) tumor compartment and (*b*) stromal compartment. [Color figure can be viewed at wileyonlinelibrary.com]

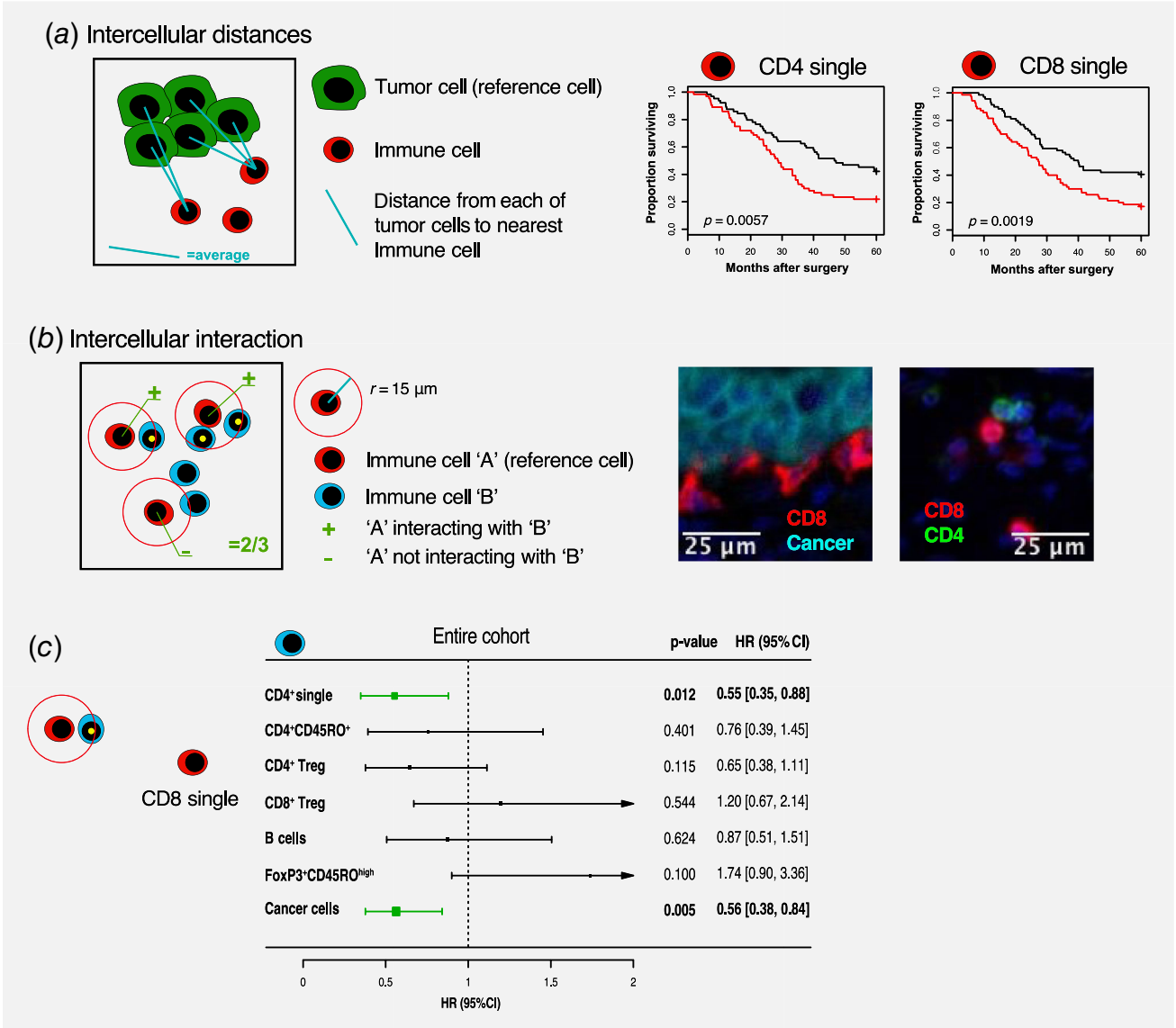

Figure 5. Spatial localization of the immune cells and their associations with survival. (*a*) A schematic illustration of the calculation of the average distance between immune cells and tumor (left) and Kaplan–Meier analysis of 5-year OS in relation to the distance of $CD4^+$ cells and $CD8^+$ cells, respectively, to tumor cells. (*b*) A schematic illustration of the calculation of the fraction of interacting cells (left). Sample immunofluorescence image illustrating $CD8^+$ cells interacting with cancer cells and $CD8^+$ cells interacting with $CD4^+$ cells. (*c*) Kaplan–Meier analysis of 5-year OS in relation to the fraction of single-positive CD8 cells interacting with other cell classes. [Color figure can be viewed at wileyonlinelibrary.com]

OS. However, none of these associations remained significant in adjusted analysis. When stratifying for tumor morphology, TN immune cell signature 3 remained significantly associated with a prolonged OS in I-type tumors, however only in relation to TN immune signature 5 (p = 0.045). This association was not confirmed in unadjusted analysis. There were no significant associations between any TN immune cell signatures and OS in PB-type tumors (Supporting Information Fig. S7).

Seven distinct stromal immune cell signatures were defined (Fig. 4*b*). Kaplan–Meier analysis revealed that in the entire cohort, stromal immune signature 5, characterized by high levels of $CD4^+CD45RO^+$ T cells, $CD8^+CD45RO^+$ T cells, B cells, $FoxP3^+CD45RO^{high}$ cells and low levels of $FoxP3^+CD45RO^{low}$ cells, was significantly associated with a prolonged OS compared to stromal immune signatures 3, 4 and 6 (p = 0.010, p = 0.011 and $p < 0.001$, respectively; Supporting Information Fig. S7). In unadjusted Cox regression analysis, using stromal immune signature 5 as a reference, stromal immune signatures 3, 4 and 6 were associated with a reduced OS (HR = 2.38, 95% CI 1.24–4.57; HR = 2.57, 95% CI 1.26–5.23; and HR = 3.09, 95% CI 1.70–5.61, respectively). These associations did not remain significant in adjusted analysis.

When stratifying for morphology, stromal immune signature 5 remained significantly associated with a prolonged OS in relation

to stromal immune signatures 3 and 6 in I-type tumors ($p = 0.019$ and $p = 0.020$; Supporting Information Fig. S7). Using stromal immune signature 5 as a reference group, stromal immune signatures 3 and 6 were significantly associated with a reduced OS in unadjusted analysis (HR = 3.84, 95% CI 1.28–11.54 and HR = 3.63, 95% CI 1.11–11.82) but not in adjusted analysis. In PB-type tumors, stromal immune signature 1, characterized by high levels of $CD8^+CD45RO^+$ T cells, B cells and single-positive CD4 cells and low levels of $FoxP3^+CD45RO^{high}$ cells and single-positive CD8 cells, was significantly associated with a prolonged OS compared to stromal immune signatures 4 and 6 ($p = 0.028$ and $p = 0.014$; Supporting Information Fig. S7). Using stromal immune signature 1 as reference group, stromal immune signatures 4 and 6 were significantly associated with a shorter OS in unadjusted Cox regression analysis (HR = 6.37, 95% CI 1.35–30.14 and HR = 4.87, 95% CI 1.1–21.58). Both signatures remained significantly associated with shorter OS in multivariable analysis (HR = 7.78, 95% CI 1.50–40.26 and HR = 6.19, 95% CI 1.35–28.37, respectively).

Spatial distribution of immune cells

In order to investigate potential interactions between TILs and cancer cells, we analyzed the distances from each cancer cell to the nearest lymphocytes (Fig. 5*a*). The strongest prognostic impact was seen for single-positive CD4 cells and single-positive $CD8^+$ cells in proximity to cancer cells (Supporting Information Fig. S8). Similar associations were found in I-type tumors, whereas in PB-type tumors, only the distance to single positive CD8 cells remained prognostic.

To delineate potential interaction mechanisms, we sought to identify direct cell-to-cell interactions of single-positive CD8 cells with other lymphocyte populations. A potential interaction event was denoted when at least one cell of another subclass was found within a 15 μm radius of a reference cell (Fig. 5*b*). The presence of single-positive CD4 cells in the interaction zone of single-positive CD8 cells was significantly associated with a prolonged survival (Fig. 5*c*). Moreover, in concordance with the above-described findings regarding average distances, the presence of cytokeratin-positive cells in the interaction zone of single positive CD8 cells was significantly associated with a prolonged survival (Fig. 5*c*).

Discussion

The inflammatory tumor microenvironment is a highly complex, heterocellular system and the concerted interactions within this system determine the anticancer immunity and most likely also the effectiveness of immunotherapy. There is, however, a lack of knowledge regarding the biological basis of the inflammatory tumor microenvironment of periampullary adenocarcinoma and the interactions herein. Our study is, to the best of our knowledge, the first effort to comprehensively map and phenotype the lymphocyte infiltration in the full spectrum of periampullary adenocarcinomas using multiplex immunofluorescence.

The results demonstrate that the infiltration of lymphocytes is dependent upon morphological subtype, with I-type tumors generally harboring higher levels of several lymphocyte subpopulations compared to PB-type tumors. The most striking immune depletion was observed in tumors of pancreatic origin, in particular in the tumor compartment. Additionally, depletion of lymphocyte infiltration was associated with several adverse clinicopathological features such as growth into lymph and blood vessels, and higher T stage. This is in contrast to a previous study using a similar multispectral method, which failed to establish any associations between T-cell infiltration and clinicopathological features in pancreatic cancer.[32] However, our study has a more detailed subclassification of lymphocytes and a different analytical approach, which may explain this disagreement.

In the present study, the infiltration of different immune cells was also evaluated separately in the stromal and tumor compartments, and the results demonstrate significant differences both in absolute values and in their prognostic implications. Such a diverse pattern of lymphocyte infiltration suggests that regulatory mechanisms may differ by tissue compartment and gives a rationale for separate analysis of immune infiltration in the tumor and stromal compartments.

When analyzing paired samples of nonmalignant tissue and primary tumors, we could demonstrate that lymphocyte infiltration was significantly higher in primary tumors, indicating an active immunological response against malignant cells. These results are in concordance with a previous report using a similar method that has demonstrated that $CD8^+$ T-cell infiltration is lower in paired benign tissue compared to tumor tissue in pancreatic cancer.[32] It must, however, be pointed out that $FoxP3^+$ cell subsets ($FoxP3^+CD45RO^{high}$ and $FoxP3^+CD45RO^{low}$ cells), that is, cells with potential immune-suppressive capacities, were among the cells with the highest predominance in tumor *versus* nontumor tissue. One explanation to this may be that human T cells can induce FoxP3 expression as a result of activation.[33]

Mutations in several genes were found to be associated with altered infiltration rates of lymphocytes. *KRAS* mutation, a very common event in pancreatic cancer, was found to be associated with lower levels of several effector T cells including single $CD8^+$ cells and $CD8^+CD45RO^+$ T cells as well as $CD8^+$ Tregs. Previously, a higher abundance of $CD4^+$ Tregs has been found to be associated with $KRAS^{G12D}$ mutations.[34] Additionally, *KRAS* mutations were found to be significantly associated with lower levels of B cells, a relationship that has not been described previously. *CDKN2A* mutations were found to be associated with lower infiltration of $CD8^+$ Tregs, which is in line with previous findings of lower levels of immune cell infiltration in a wide range of solid tumors with *CDKN2A* mutation, including pancreatic cancer.[35] Mutations in *SMAD4* and *APC* were found to be associated with higher abundance of several $CD8^+$ lymphocyte subsets and in the case of *APC* also with $CD4^+$ lymphocytes. In I-type tumors, dMMR status was

associated with higher lymphocyte infiltration. It has previously been shown, with single stain immunohistochemistry, that $CD8^+$ T cells are more abundant in dMMR I-type tumors,[26] but the present study provides a much more detailed phenotyping. dMMR leads to hypermutation and increased neoepitope formation,[36] in turn potentially leading to a more efficient immunological response and increased infiltration of immune cells into the tumor. This association was not seen in PB-type tumors, which is in line with previous findings in pancreatic cancer.[37]

Several associations were observed between certain lymphocyte subpopulations and survival. Of particular interest were $CD8^+$ cell subsets, which demonstrated consistent associations with a prolonged survival. In particular, activated and/or memory $CD8^+$ T cells (i.e. $CD8\alpha^+CD45RO^+$), but not single-positive CD8 cells, were prognostic when analyzed as total cell density. One should, however, be cautious when drawing conclusions from these data. The distinction between activated and/or memory and single-positive CD8 cells was made by applying a cut-off for the CD45RO expression, and it must be pointed out that this protein has a continuous expression in lymphocytes, potentially reflecting a continuum of the activation status of $CD8^+$ cells. Identifying a proper methodology for handling this biological complexity is a matter of further studies.

Of note, Tregs ($CD4^+FoxP3^+$), commonly suggested to be immune inhibitory, were not associated with adverse patient outcome in our study. These data are in line with previous research in pancreatic cancer[25] and lung cancer,[32] suggesting other immune inhibitory mechanisms. Also, it may indicate that FoxP3 expression in tumors can be induced by activation *per se*, without being linked to an immunosuppressive function.[33] This hypothesis is in concordance with a previous study by Stromnes *et al.*, demonstrating that FoxP3 levels on Tregs from pancreatic tumor tissue were significantly higher than on Tregs in adjacent benign tissue,[21] possibly indicating that FoxP3 is elevated due to activation. This observation may be important for understanding the mechanisms underlying immune evasion in periampullary adenocarcinomas.

Further, the present study identified several immune cell infiltration signatures that were significantly associated with survival, many sharing the common characteristic of having comparatively high levels of $CD4^+CD45RO^+$ and $CD8^+CD45RO^+$ T cells and $FoxP3^+CD45RO^{high}$ cells. Interestingly, in the stromal compartment, the signatures that were found to be prognostic also had high levels of B cells. Several differences were also identified between the two morphologies regarding the prognostic impact of the defined immune cell signatures. Notably, stromal immune cell signature 5 (characterized by high levels of $CD4^+CD45RO^+$ and $CD8^+CD45RO^+$ T cells, $FoxP3^+CD45RO^{high}$ and B cells, but low levels of $FoxP3^+CD45RO^{low}$ cells) was significantly associated with a prolonged survival only for patients with I-type tumors, and this survival benefit was retained against most of the other defined stromal immune cell signatures. In mice and in *in vitro* studies, FoxP3 has been shown to be expressed in tumor promoting, immunosuppressive macrophages and dendritic cells as well,[38,39] whether this may also be the case in humans is as of today not yet known, but will be interesting to follow.

As noted above, stromal immune cell signature 5 was defined by high density of $FoxP3^+CD45RO^{high}$ cells but low density of $FoxP3^+CD45RO^{low}$ cells, which could, at least partly, represent a naïve Treg population,[40] indicating a different functionality between these distinct $FoxP3^+$ cell populations in I-type tumors. Previously, it has been shown that activated/memory Tregs and naïve Tregs have the same suppressive capabilities,[41] therefore one could speculate that the functionality does not lie in the $FoxP3^+$ cell populations themselves, but rather in the interplay between the $FoxP3^+$ cell populations and other immune cells, which have been shown to be of prognostic value in previous studies.[32,42,43] In PB-type tumors, stromal immune cell signature 1, and not 5, was associated with a prolonged survival, and this association remained significant even after adjustment for clinicopathological factors. Stromal immune cell signatures 1 and 5 were similar in composition, but in contrast to stromal immune cell signature 5, stromal immune cell signature 1 was also characterized by low levels of $FoxP3^+CD45RO^{high}$ cells. This could imply that there is a difference between the two morphologies regarding which immune cells constitute an effective antitumor response. The results from our study indicate that there is a subgroup of patients with immunogenic tumors with low levels of immunosuppressive lymphocytes but high levels of effector lymphocytes, and that these patients have a better prognosis. These results are in line with previous research in pancreatic cancer.[32,44]

Finally, we investigated spatial localization of the immune cells in relation to tumor cells and to other lymphocyte subpopulations. We identified single-positive $CD8^+$ cells being of particular importance when localized in immediate vicinity to cancer cells. We managed to demonstrate this observation by different methods, evaluating single-positive $CD8^+$ cell enrichment in the tumor *versus* stromal compartment, and by analyzing their potential direct interaction with cancer cells. The potential interaction zone between lymphocytes was set to a radius of 15 μm, based on previous publications, indicating 15 μm to be most appropriate distance to analyze potentially predictive features of cell-to-cell interactions.[45] Overall, our results demonstrate that single-positive CD8 cell interaction with cancer cells is an independent prognostic factor in periampullary adenocarcinoma. These findings are in line with previous studies on pancreatic cancer.[32,46] A recent study by Masugi *et al.*, could not establish a significant association between $CD8^+$ T-cell proximity to cancer cells and patient survival, however, our study used a different methodology.[47] They did, however, find a significant association between patient survival and $CD8^+$ T-cell infiltration in the tumor center, further supporting that the topographic infiltration patterns of $CD8^+$ cells are of prognostic importance.[47] Further,

the *in situ* cell mapping allowed us to identify a potential interaction between single-positive $CD8^+$ cells and $CD4^+$ cells. Although the particular mechanism behind this observation remains unknown, it has been reported that $CD4^+$ cells can be helpful for the $CD8^+$ cell recruitment, proliferation and effector function within the tumor nest by producing IFN-γ and IL-2.[48–50] Another mechanism could be through the cooperation between $CD8^+$ and $CD4^+$ cells for the bystander killing of cancer through targeting of stromal cells.[51] This is, to the best of our knowledge, the first such observation in the *in situ* environment of cancer tissue.

Conclusions

The present study provides a first detailed description of the lymphocyte infiltration patterns in periampullary adenocarcinoma. The data presented demonstrate that the composition, topography and clinical impact of lymphocyte infiltration differ by morphological type as well as by localization. The multiplex technique with spatial cell mapping indicates specific mechanisms of the immune regulation in human tumors, and the findings may help to stratify patients in the context of immunotherapy or suggest combined modalities to overcome resistance.

Acknowledgements

This work was supported by grants from the Swedish Cancer Society, the Swedish Research Council; the Swedish Government Grant for Clinical Research, the Mrs Berta Kamprad Foundation, the Sjöberg Foundation, BioCARE, Lund University Faculty of Medicine, the Erik, Karin och Gösta Selanders Stiftelse and Skåne University Hospital Research Grants.

Conflict of interest

The authors declare that they have no conflict of interest.

References

1. He C, Mao Y, Wang J, et al. Surgical management of periampullary adenocarcinoma: defining an optimal prognostic lymph node stratification schema. *J Cancer* 2018;9:1667–79. https://doi.org/10.7150/jca.24109.
2. Westgaard A, Tafjord S, Farstad IN, et al. Pancreatobiliary versus intestinal histologic type of differentiation is an independent prognostic factor in resected periampullary adenocarcinoma. *BMC Cancer* 2008;8:170. https://doi.org/10.1186/1471-2407-8-170.
3. Bronsert P, Kohler I, Werner M, et al. Intestinal-type of differentiation predicts favourable overall survival: confirmatory clinicopathological analysis of 198 periampullary adenocarcinomas of pancreatic, biliary, ampullary and duodenal origin. *BMC Cancer* 2013;13:428. https://doi.org/10.1186/1471-2407-13-428.
4. Kimura W, Futakawa N, Zhao B. Neoplastic diseases of the papilla of Vater. *J Hepatobiliary Pancreat Surg* 2004;11:223–31. https://doi.org/10.1007/s00534-004-0894-7.
5. Lundgren S, Hau SO, Elebro J, et al. Mutational landscape in resected Periampullary adenocarcinoma: relationship with morphology and clinical outcome. *JCO Precis Oncol* 2019;3:1–8. https://doi.org/10.1200/Po.18.00323.
6. Ilic M, Ilic I. Epidemiology of pancreatic cancer. *World J Gastroenterol* 2016;22:9694–705. https://doi.org/10.3748/wjg.v22.i44.9694.
7. Vincent A, Herman J, Schulick R, et al. Pancreatic cancer. *Lancet (London, England)* 2011;378:607–20. https://doi.org/10.1016/s0140-6736(10)62307-0.
8. Burris HA 3rd, Moore MJ, Andersen J, et al. Improvements in survival and clinical benefit with gemcitabine as first-line therapy for patients with advanced pancreas cancer: a randomized trial. *J Clin Oncol* 1997;15:2403–13. https://doi.org/10.1200/jco.1997.15.6.2403.
9. Conroy T, Desseigne F, Ychou M, et al. FOLFIRINOX versus gemcitabine for metastatic pancreatic cancer. *N Engl J Med* 2011;364:1817–25. https://doi.org/10.1056/NEJMoa1011923.
10. Conroy T, Hammel P, Hebbar M, et al. FOLFIRINOX or gemcitabine as adjuvant therapy for pancreatic cancer. *N Engl J Med* 2018;379:2395–406. https://doi.org/10.1056/NEJMoa1809775.
11. Hanahan D, Weinberg RA. Hallmarks of cancer: the next generation. *Cell* 2011;144:646–74. https://doi.org/10.1016/j.cell.2011.02.013.
12. Badalamenti G, Fanale D, Incorvaia L, et al. Role of tumor-infiltrating lymphocytes in patients with solid tumors: can a drop dig a stone? *Cell Immunol* 2018;343:103753. https://doi.org/10.1016/j.cellimm.2018.01.013.
13. Galon J, Costes A, Sanchez-Cabo F, et al. Type, density, and location of immune cells within human colorectal tumors predict clinical outcome. *Science (New York, NY)* 2006;313:1960–4. https://doi.org/10.1126/science.1129139.
14. Pages F, Galon J, Dieu-Nosjean MC, et al. Immune infiltration in human tumors: a prognostic factor that should not be ignored. *Oncogene* 2010;29:1093–102. https://doi.org/10.1038/onc.2009.416.
15. Foucher ED, Ghigo C, Chouaib S, et al. Pancreatic ductal adenocarcinoma: a strong imbalance of good and bad immunological cops in the tumor microenvironment. *Front Immunol* 2018;9:1044. https://doi.org/10.3389/fimmu.2018.01044.
16. Mahajan UM, Langhoff E, Goni E, et al. Immune cell and stromal signature associated with progression-free survival of patients with resected pancreatic ductal adenocarcinoma. *Gastroenterology* 2018;155:1625–1639.e2. https://doi.org/10.1053/j.gastro.2018.08.009.
17. Beatty GL, Gladney WL. Immune escape mechanisms as a guide for cancer immunotherapy. *Clin Cancer Res* 2015;21:687–92. https://doi.org/10.1158/1078-0432.Ccr-14-1860.
18. Kabacaoglu D, Ciecielski KJ, Ruess DA, et al. Immune checkpoint inhibition for pancreatic ductal adenocarcinoma: current limitations and future options. *Front Immunol* 2018;9:1878. https://doi.org/10.3389/fimmu.2018.01878.
19. Danilova L, Ho WJ, Zhu Q, et al. Programmed cell death ligand-1 (PD-L1) and CD8 expression profiling identify an immunologic subtype of pancreatic ductal adenocarcinomas with favorable survival. *Cancer Immunol Res* 2019;7:886–95. https://doi.org/10.1158/2326-6066.Cir-18-0822.
20. Bailey P, Chang DK, Nones K, et al. Genomic analyses identify molecular subtypes of pancreatic cancer. *Nature* 2016;531:47–52. https://doi.org/10.1038/nature16965.
21. Stromnes IM, Hulbert A, Pierce RH, et al. T-cell localization, activation, and clonal expansion in human pancreatic ductal adenocarcinoma. *Cancer Immunol Res* 2017;5:978–91. https://doi.org/10.1158/2326-6066.Cir-16-0322.
22. Herbst RS, Soria JC, Kowanetz M, et al. Predictive correlates of response to the anti-PD-L1 antibody MPDL3280A in cancer patients. *Nature* 2014;515:563–7. https://doi.org/10.1038/nature14011.
23. Taube JM, Klein A, Brahmer JR, et al. Association of PD-1, PD-1 ligands, and other features of the tumor immune microenvironment with response to anti-PD-1 therapy. *Clin Cancer Res* 2014;20:5064–74. https://doi.org/10.1158/1078-0432.Ccr-13-3271.
24. Elebro J, Jirstrom K. Use of a standardized diagnostic approach improves the prognostic information of histopathologic factors in pancreatic and periampullary adenocarcinoma. *Diagn Pathol* 2014;9:80. https://doi.org/10.1186/1746-1596-9-80.
25. Elebro J, Heby M, Warfvinge CF, et al. Expression and prognostic significance of human epidermal growth factor receptors 1, 2 and 3 in Periampullary adenocarcinoma. *PLoS One* 2016;11:e0153533. https://doi.org/10.1371/journal.pone.0153533.
26. Heby M, Lundgren S, Nodin B, et al. Relationship between mismatch repair immunophenotype and long-term survival in patients with resected periampullary adenocarcinoma. *J Transl Med* 2018;16:66. https://doi.org/10.1186/s12967-018-1444-4.
27. Elebro J, Heby M, Gaber A, et al. Prognostic and treatment predictive significance of SATB1 and SATB2 expression in pancreatic and periampullary adenocarcinoma. *J Transl Med* 2014;12:289. https://doi.org/10.1186/s12967-014-0289-8.

28. Heby M, Elebro J, Nodin B, et al. Prognostic and predictive significance of podocalyxin-like protein expression in pancreatic and periampullary adenocarcinoma. *BMC Clin Pathol* 2015;15:10. https://doi.org/10.1186/s12907-015-0009-1.
29. Mezheyeuski A, Bergsland CH, Backman M, et al. Multispectral imaging for quantitative and compartment-specific immune infiltrates reveals distinct immune profiles that classify lung cancer patients. *J Pathol* 2018;244:421–31. https://doi.org/10.1002/path.5026.
30. Karanikas V, Speletas M, Zamanakou M, et al. Foxp3 expression in human cancer cells. *J Transl Med* 2008;6:19. https://doi.org/10.1186/1479-5876-6-19.
31. Martin F, Ladoire S, Mignot G, et al. Human FOXP3 and cancer. *Oncogene* 2010;29:4121–9. https://doi.org/10.1038/onc.2010.174.
32. Carstens JL, de Sampaio PC, Yang D, et al. Spatial computation of intratumoral T cells correlates with survival of patients with pancreatic cancer. *Nat Commun* 2017;8:15095. https://doi.org/10.1038/ncomms15095.
33. Kmieciak M, Gowda M, Graham L, et al. Human T cells express CD25 and Foxp3 upon activation and exhibit effector/memory phenotypes without any regulatory/suppressor function. *J Transl Med* 2009;7:89. https://doi.org/10.1186/1479-5876-7-89.
34. Cheng H, Fan K, Luo G, et al. Kras(G12D) mutation contributes to regulatory T cell conversion through activation of the MEK/ERK pathway in pancreatic cancer. *Cancer Lett* 2019;446:103–11. https://doi.org/10.1016/j.canlet.2019.01.013.
35. Siemers NO, Holloway JL, Chang H, et al. Genome-wide association analysis identifies genetic correlates of immune infiltrates in solid tumors. *PLoS One* 2017;12:e0179726. https://doi.org/10.1371/journal.pone.0179726.
36. Dudley JC, Lin MT, Le DT, et al. Microsatellite instability as a biomarker for PD-1 blockade. *Clin Cancer Res* 2016;22:813–20. https://doi.org/10.1158/1078-0432.Ccr-15-1678.
37. Tessier-Cloutier B, Kalloger SE, Al-Kandari M, et al. Programmed cell death ligand 1 cut-point is associated with reduced disease specific survival in resected pancreatic ductal adenocarcinoma. *BMC Cancer* 2017;17:618. https://doi.org/10.1186/s12885-017-3634-5.
38. Zorro Manrique S, Duque Correa MA, Hoelzinger DB, et al. Foxp3-positive macrophages display immunosuppressive properties and promote tumor growth. *J Exp Med* 2011;208:1485–99. https://doi.org/10.1084/jem.20100730.
39. Lipscomb MW, Taylor JL, Goldbach CJ, et al. DC expressing transgene Foxp3 are regulatory APC. *Eur J Immunol* 2010;40:480–93. https://doi.org/10.1002/eji.200939667.
40. Miyara M, Yoshioka Y, Kitoh A, et al. Functional delineation and differentiation dynamics of human CD4+ T cells expressing the FoxP3 transcription factor. *Immunity* 2009;30:899–911. https://doi.org/10.1016/j.immuni.2009.03.019.
41. Booth NJ, McQuaid AJ, Sobande T, et al. Different proliferative potential and migratory characteristics of human CD4+ regulatory T cells that express either CD45RA or CD45RO. *J Immunol* 2010;184:4317–26. https://doi.org/10.4049/jimmunol.0903781.
42. Feichtenbeiner A, Haas M, Buttner M, et al. Critical role of spatial interaction between CD8(+) and Foxp3(+) cells in human gastric cancer: the distance matters. *Cancer Immunol Immunother* 2014;63:111–9. https://doi.org/10.1007/s00262-013-1491-x.
43. Barua S, Fang P, Sharma A, et al. Spatial interaction of tumor cells and regulatory T cells correlates with survival in non-small cell lung cancer. *Lung Cancer (Amsterdam, Netherlands)* 2018;117:73–9. https://doi.org/10.1016/j.lungcan.2018.01.022.
44. Wartenberg M, Cibin S, Zlobec I, et al. Integrated genomic and Immunophenotypic classification of pancreatic cancer reveals three distinct subtypes with prognostic/predictive significance. *Clin Cancer Res* 2018;24:4444–54. https://doi.org/10.1158/1078-0432.Ccr-17-3401.
45. Schwen LO, Andersson E, Korski K, et al. Data-driven discovery of immune contexture biomarkers. *Front Oncol* 2018;8:627. https://doi.org/10.3389/fonc.2018.00627.
46. Barua S, Solis L, Parra ER, et al. A functional spatial analysis platform for discovery of immunological interactions predictive of low-grade to high-grade transition of pancreatic Intraductal papillary mucinous neoplasms. *Cancer informatics* 2018;17:1176935118782880. https://doi.org/10.1177/1176935118782880.
47. Masugi Y, Abe T, Ueno A, et al. Characterization of spatial distribution of tumor-infiltrating CD8 (+) T cells refines their prognostic utility for pancreatic cancer survival. *Mod Pathol* 2019;32:1495–507. https://doi.org/10.1038/s41379-019-0291-z.
48. Giuntoli RL 2nd, Lu J, Kobayashi H, et al. Direct costimulation of tumor-reactive CTL by helper T cells potentiate their proliferation, survival, and effector function. *Clin Cancer Res* 2002;8:922–31.
49. Bos R, Sherman LA. CD4+ T-cell help in the tumor milieu is required for recruitment and cytolytic function of CD8+ T lymphocytes. *Cancer Res* 2010;70:8368–77. https://doi.org/10.1158/0008-5472.Can-10-1322.
50. Bos R, Marquardt KL, Cheung J, et al. Functional differences between low- and high-affinity CD8(+) T cells in the tumor environment. *Oncoimmunology* 2012;1:1239–47. https://doi.org/10.4161/onci.21285.
51. Schietinger A, Philip M, Liu RB, et al. Bystander killing of cancer requires the cooperation of CD4 (+) and CD8(+) T cells during the effector phase. *J Exp Med* 2010;207:2469–77. https://doi.org/10.1084/jem.20092450.